NANO LETTERS

2003
Vol. 3, No. 7
939−943

Dichroic Optical Properties of Extended Nanostructures Fabricated Using Angle-Resolved Nanosphere Lithography

Christy L. Haynes and Richard P. Van Duyne*

Department of Chemistry, Northwestern University, 2145 Sheridan Road, Evanston, Illinois 60208-3113

Received April 15, 2003; Revised Manuscript Received May 5, 2003

ABSTRACT

Extended angle-resolved noble metal nanostructures such as nanooverlaps, nanocontacts, nanogaps, and nanochains show diverse optical characteristics. Polarized microextinction spectroscopy demonstrates dichroic contrast varying between 20 and 200 nm upon comparing the optical spectra of the transverse and longitudinal localized surface plasmon resonance modes. This dichroic contrast can be easily controlled by regulating deposition conditions.

Nanotechnology research is driven by the demand for ever smaller device features needed to achieve improved performance and decreased cost in the microelectronics, optical communications, and data storage industries. Developments in nanotechnology rely on the design and fabrication of nanostructures with features in the 1−100 nm size regime. The ideal nanofabrication technique would be materials- and substrate-general, inexpensive, flexible in nanoparticle size, shape, and spacing parameters, and massively parallel. Several standard lithographic methods are routinely used to create nanostructures with controlled size, shape, and interparticle spacing with varying success.[1−8]

Many nanofabrication techniques aim to create high aspect ratio nanoparticles or nanoparticle assemblies so that the materials may be applied as dichroic filters. The dichroic behavior results from the excitation of the size-dependent localized surface plasmon resonance (LSPR) of the vastly different nanoparticle dimensions present in high aspect ratio nanoparticles. For example, Aussenegg and co-workers used electron beam lithography to define high aspect ratio Ag nanorods for dichroic applications.[9] Upon changing the polarization of the exciting light from parallel to the long axis of the nanorods to perpendicular to the long axis of the nanorods, the LSPR shifted from 600 to 420 nm. Foss and co-workers distributed both spherical and cylindrical Au nanoparticles into oriented polyethylene films, generating stripes of nanoparticles.[10,11] The dichroic behavior was apparent upon varying the nanoparticle assembly orientation relative to a polarized excitation source. In fact, the LSPR shifted from 700 to 545 nm in the most extreme case. The LSPR spectra differ drastically in both extinction maximum and width when exciting parallel and perpendicular to the long axis of the oriented nanoparticles. In a similar experiment, Dirix and co-workers show color images of Ag nanoparticles embedded and oriented in polyethylene films in both polarization matching conditions.[12] When the polarized excitation is parallel to the oriented nanoparticle stripes, the film appears red in color; polarized excitation perpendicular to the oriented nanoparticle stripes yields a yellow film. In recent work, Fort and co-workers controlled the growth of Ag nanowires on facetted aluminum substrates to create high aspect ratio nanostructures.[13] Excitation of the transverse and longitudinal LSPRs yield optical spectra that vary by almost 100 nm in extinction maximum. While each of these nanofabrication methods holds potential for producing marketable dichroic materials, the ideal nanofabrication technique would flexibly create nanostructures so that the dichroic contrast between the longitudinal and transverse LSPR spectra could be easily tuned. This work demonstrates that a simple variant of nanosphere lithography presents this opportunity.

Conventional nanosphere lithography (NSL) begins with the self-assembly of a nanosphere mask of a given diameter, *D*, onto a substrate followed by line-of-sight deposition of a material(s) through the mask.[14,15] In general, the substrate to be patterned is positioned normal to the direction of material deposition. The resultant nanoparticles have an in-plane shape and interparticle spacing determined by the projection of the nanosphere mask interstices onto the substrate. A monolayer mask produces nanoparticles having a triangular in-plane shape arranged on the surface with P_6mm symmetry. The ratio of the interparticle spacing to the in-plane perpendicular bisector is a fixed value, ca. 2.5.

* Corresponding author. E-mail: vanduyne@chem.northwestern.edu.

10.1021/nl0342287 CCC: $25.00
Published on Web 05/24/2003

In previous work, we reported a novel fabrication technique that is a simple variant on conventional NSL, known as angle-resolved nanosphere lithography (AR NSL).[16] AR NSL produces vastly different and increasingly flexible nanostructures by controlling the angle between the surface normal of the sample assembly and the propagation vector of the material deposition beam (θ). The nanosphere mask registry (ϕ) also affects the resultant nanostructure. All previous AR NSL work exploited nanostructures fabricated by performing a single noble metal deposition through the nanosphere mask. The range of accessible structural motifs can be further expanded by performing a series of material depositions on the same sample under AR NSL conditions.

Two-dimensional colloidal crystal masks were assembled as described in previous work.[16] The metal films were deposited in a modified consolidated vacuum corporation vapor deposition system[17] with a base pressure of 10^{-7} Torr. The mass thickness, d_m, and deposition rate for each film were measured using a Leybold Inficon XTM/2 quartz-crystal microbalance. Samples were mounted 240 mm above the effusive source with three 25 mm diameter apertures regularly spaced between the source and the sample to provide collimation of the physical vapor deposition beam. θ, the angle between the surface normal of the sample assembly and the propagation vector of the material deposition beam, was controlled by mounting the samples on machined Al blocks. Extended AR NSL nanostructures were fabricated by removing the nanosphere mask from the vacuum chamber after each deposition to remount the nanosphere mask on the desired θ-defining block. After all metal depositions were complete, removal of the polystyrene nanospheres was achieved by sonication in absolute ethanol for 3 min.

Many complex nanostructures are accessible using the multiple deposition AR NSL technique. For example, consider mounting a 400 nm diameter nanosphere mask onto a precision-machined aluminum 15° angle block, depositing 20 nm of Ag metal, and then moving the sample onto a 22° angle block and depositing another 20 nm of Ag metal. After removing the nanospheres, the resultant nanostructure will consist of periodic sets of two nonequilateral triangular footprints that overlap one another. The footprint of each individual nanoparticle is determined by both the ϕ angle of a given domain and the overall θ angle, as described by a simple geometric model presented in previous work.[16] The extent of nanoparticle overlap is determined by the relationship between the two chosen θ angles. Figure 1 demonstrates the four major motifs accessible by implementing multiple deposition AR NSL. When there is a small difference in the θ angles of two depositions, a nanooverlap structure results; Figure 1A was fabricated with $D = 400$ nm, $\theta_1 = 0°$, $d_{m1} = 15$ nm Ag, $\theta_2 = 17.5°$, and $d_{m2} = 35$ nm Ag. When the two θ angles fulfill the correct geometric condition, a nanocontact structure results; Figure 1B was fabricated with $D = 400$ nm, $\theta_1 = 0°$, $d_{m1} = 15$ nm Ag, $\theta_2 = 23.5°$, and $d_{m2} = 35$ nm Ag. When there is a large difference in the θ angles of two depositions, a nanogap structure results; Figure 1C was fabricated with $D = 400$ nm, $\theta_1 = 0°$, $d_{m1} = 30$ nm Ag, $\theta_2 = 30°$, and $d_{m2} = 30$ nm Ag. Finally, it is possible to further extend the library of accessible nanostructures by performing more than two depositions under varied θ and ϕ angles. Figure 1D shows a nanochain structure fabricated with $D = 400$ nm, $\theta_1 = 0°$, $d_{m1} = 15$ nm Ag, $\theta_2 = 15°$, $d_{m2} = 15$ nm Ag, $\theta_3 = -15°$, and $d_{m3} = 15$ nm Ag. In this case, a negative θ value signifies that the angle block has been rotated 180° in the plane normal to the effusive deposition beam.

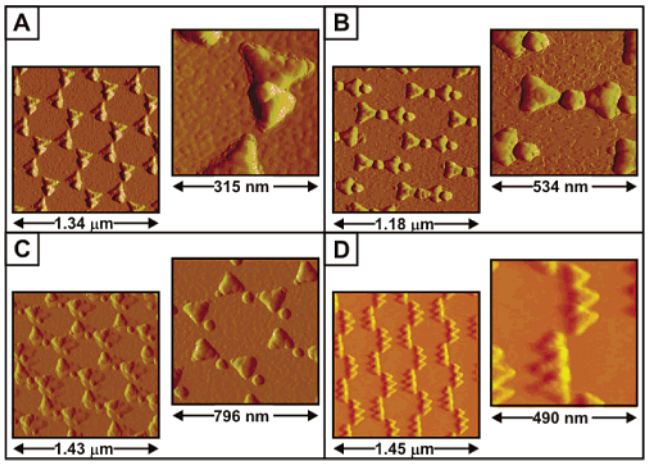

Figure 1. Atomic force microscopy images of multiple deposition angle-resolved nanosphere lithography structures. (A) Nanooverlap structures fabricated using nanospheres with $D = 400$ nm, $\theta_1 = 0°$, $d_{m1} = 15$ nm Ag, $\theta_2 = 17.5°$, $d_{m2} = 35$ nm Ag. (B) Nanocontact structures fabricated using nanospheres with $D = 400$ nm, $\theta_1 = 0°$, $d_{m1} = 15$ nm Ag, $\theta_2 = 23.5°$, $d_{m2} = 35$ nm Ag. (C) Nanogap structures fabricated using nanospheres with $D = 400$ nm, $\theta_1 = 0°$, $d_{m1} = 30$ nm Ag, $\theta_2 = 30°$, $d_{m2} = 30$ nm Ag. (D) Nanochain structures fabricated using nanospheres with $D = 400$ nm, $\theta_1 = 0°$, $d_{m1} = 15$ nm Ag, $\theta_2 = 15°$, $d_{m2} = 15$ nm Ag, $\theta_3 = -15°$, $d_{m3} = 15$ nm Ag.

While the LSPR spectra of single deposition AR NSL nanostructures look very similar to those of standard NSL nanostructures,[18−24] multiple deposition AR NSL nanostructures demonstrate diverse LSPR characteristics. This alternative spectroscopic behavior was expected due to the close spatial proximity of the nanoparticles that result from each individual deposition in the series of depositions, as well as the high aspect ratio character of resultant nanostructure. Polarized microextinction spectroscopy was implemented in order to fully probe the optical properties of the extended AR NSL nanostructures. Spatially resolved polarized microextinction spectra were measured using a modified Nikon Optiphot confocal microscope with a 20× objective in backscattering geometry. The nanostructure sample was placed on a mirrored rotation mount that was centered under the objective so that no sample translation occurred during rotation. A polarizing filter was placed in fixed position before the microscope objective. When recording an extinction spectrum, the light from a tungsten−halogen lamp was coupled into a 200 μm core diameter fiber using a fiber launch, and the output fiber optic was coupled to an Ocean Optics model SD2000 spectrometer. The illumination spot size was ~25 μm in diameter.

In all cases, the polarization of the white light impinging upon the nanostructures was fixed based on the position of

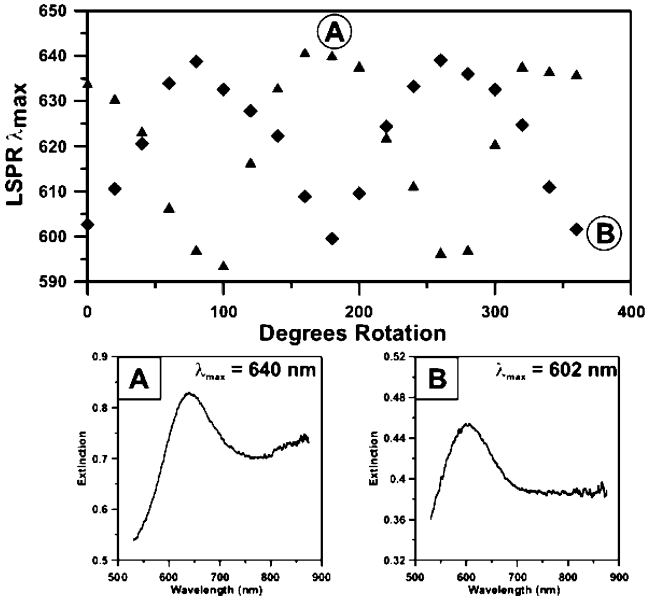

Figure 2. Polarized microextinction of Ag nanooverlap structure. In this example, $\theta_1 = 0°$, $d_{m1} = 30$ nm and $\theta_2 = 6°$, $d_{m2} = 30$ nm. LSPR λ_{max} values were measured with vertically (diamonds) and horizontally (triangles) polarized excitation. Insets (A) and (B) show example extinction spectra.

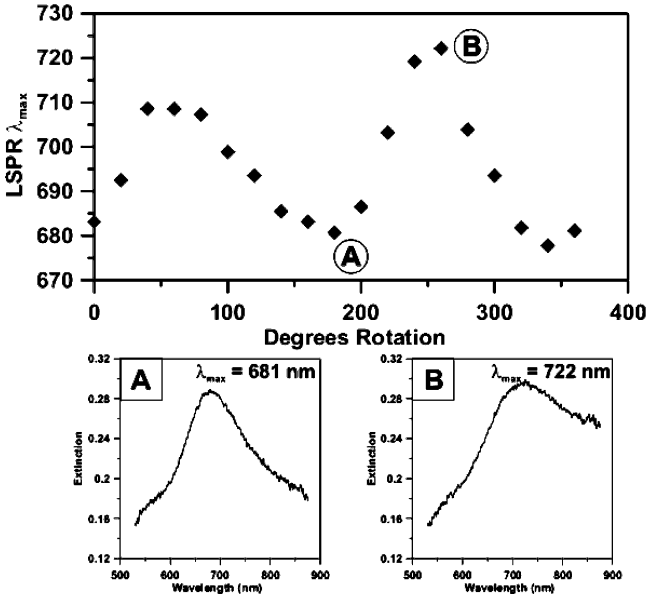

Figure 3. Polarized microextinction of Ag nanocontact structure. In this example, $\theta_1 = 0°$, $d_{m1} = 30$ nm and $\theta_2 = 20°$, $d_{m2} = 30$ nm; LSPR λ_{max} values were measured with vertically polarized excitation. Insets (A) and (B) show example extinction spectra.

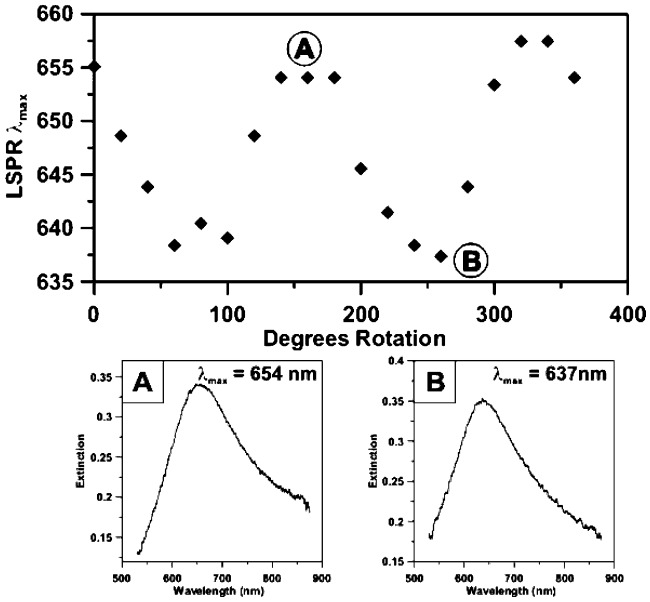

Figure 4. Polarized microextinction of Ag nanogap structure. In this example, $\theta_1 = 0°$, $d_{m1} = 30$ nm and $\theta_2 = 23.5°$, $d_{m2} = 30$ nm; LSPR λ_{max} values were measured with vertically polarized excitation. Insets (A) and (B) show example extinction spectra.

the polarizing filter, and the sample was rotated relative to this fixed polarization. The starting position of the sample relative to the impinging polarized light was arbitrary; extinction spectra were recorded after each 20° turn in the rotation mount. Figure 2 shows the polarized microextinction behavior of the nanooverlap motif. The spectral location of the extinction maximum, λ_{max}, is shown as a function of sample rotation with both vertical (diamonds) and horizontal (triangles) polarization. In this case, the extinction maximum oscillates between values of 594 and 641 nm depending on the orientation of the sample relative to the impinging light. There is 180° periodicity, and the vertical and horizontal excitation cases illustrate equal and opposite maxima and minima as expected. In this case, the periodic sets of two nonequilateral triangular footprints that overlap one another are electromagnetically coupled and acting as one large, high aspect ratio (viz., 1.45) nanoparticle. When the polarization of the excitation light is coincident with the long axis of the nanoparticles, the extinction maximum occurs at longer wavelength values. Meanwhile, when the polarization of the excitation light is coincident with the short axis of the nanoparticles, the extinction maximum occurs at shorter wavelength values. Because the nanostructure behaves as periodic rod-like nanoparticles, 2-fold symmetry in the extinction behavior is expected. Example extinction spectra are shown in Figures 2A and 2B.

Figure 3 shows the polarized microextinction behavior of the nanocontact motif. The spectral location of the extinction maximum is shown as a function of sample rotation with vertical polarization. In this case, the extinction maximum oscillates between values of 678 and 724 nm with 2-fold symmetry, depending on the orientation of the sample relative to the impinging light. In the nanocontact motif, the periodic sets of two nonequilateral triangular footprints are just touching one another and, accordingly, act as one large, high aspect ratio (viz., 2) nanoparticle. Example extinction spectra are shown in Figures 3A and 3B.

Figure 4 shows the polarized microextinction behavior of the nanogap motif. The spectral location of the extinction maximum is shown as a function of sample rotation with vertical polarization. In this case, the extinction maximum oscillates between values of 637 and 657 nm with 2-fold symmetry, depending on the orientation of the sample relative to the impinging light. While it is apparent that both the nanooverlap and nanocontact structures act as large, elec-

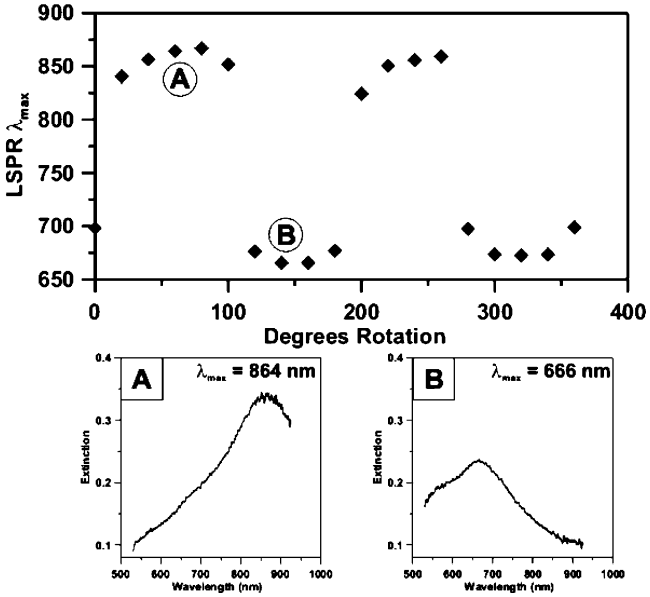

Figure 5. Polarized microextinction of Ag nanochain structure. In this example, $\theta_1 = 0°$, $d_{m1} = 30$ nm, $\theta_2 = 15°$, $d_{m2} = 30$ nm, and $\theta_3 = -15°$, $d_{m3} = 30$ nm; LSPR λ_{max} values were measured with vertically polarized excitation. Insets (A) and (B) show example extinction spectra.

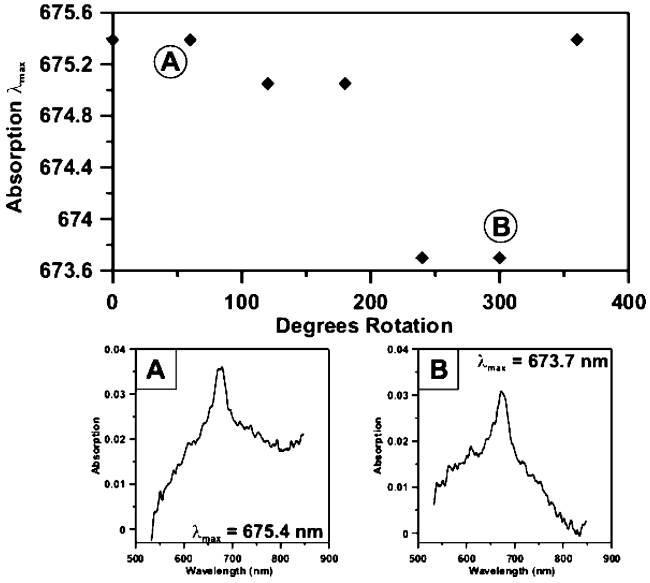

Figure 6. Polarized microextinction of cobalt phthalocyanine control. The solution of 5 mM cobalt phthalocyanine in pyridine was probed with vertically polarized excitation (integration time = 1000 ms, avg = 3, boxcar = 3). Insets (A) and (B) show example absorption spectra.

tromagnetically coupled nanorods, the nanogap structures (overall aspect ratio = 2.2) shows more complex optical behavior. While the 2-fold symmetry in the extinction maximum is still apparent, the magnitude of the difference between the minimum and maximum values is significantly decreased (i.e., 20 nm for the nanogap versus 47 nm for the nanocontact). This apparent lack of polarization contrast was ubiquitous in nanogap samples and can be attributed to the complicated nature of electromagnetic coupling. This phenomenon has been recently discussed in related work.[25] Example extinction spectra are shown in Figures 4A and 4B.

Figure 5 shows the polarized microextinction behavior of the nanochain motif. The spectral location of the extinction maximum is shown as a function of sample rotation with vertical polarization. In this case, the polarization contrast is very large as the extinction maximum oscillates between values of 666 and 864 nm with 2-fold symmetry. Features in the nanochain motif behave as extended nanocontact samples; the periodic sets of three nonequilateral triangular footprints are overlapping one another and, accordingly, act as one large, high aspect ratio (viz., 3) nanoparticle. Example extinction spectra are shown in Figures 5A and 5B. It is interesting to note that the extinction maximum versus sample rotation plot reveals nearly square wave behavior instead of the sinusoidal behavior measured in all other cases. While observing the extinction spectra during sample rotation, it is clear that, unlike the spectral trends for lower aspect ratio nanostructures, the extinction peak does not progress smoothly from low energy to high energy and vice versa. Instead, these high aspect ratio nanochains behave as one would expect infinite Ag nanowires to behave, revealing only one LSPR mode or the other. In this high aspect ratio case, it is clear that the longitudinal and transverse LSPR modes are not simultaneously excited.

A control experiment was done with a cobalt phthalocyanine (CoPc) solution to verify that the 180° symmetry measured in all cases was not an instrumental artifact. The 5 mM solution of CoPc in pyridine was placed in a thin cell beneath the microscope objective. The absorbing molecules in solution should show no polarization dependence. Figure 6 shows the polarized microextinction behavior of the CoPc solution as well as two example spectra. The absorption λ_{max} varies by less than 2 nm during sample rotation, demonstrating that the 2-fold symmetry is not an artifact.

Attempts were made to correlate nanostructure aspect ratio to the magnitude of the difference between the minimized λ_{max} (short axis coincident with polarization direction) and the maximized λ_{max} (long axis coincident with polarization direction). Due to the complicated behavior of the nanogap motif, this was not possible. When considering this relationship for just the three nanostructures that demonstrate efficient electromagnetic coupling between the individual constituents of the nanostructure, a linear relationship is apparent. As expected, increased aspect ratio yields an increased difference between the minimized and maximized λ_{max} values. Specifically, a 1 unit increase in nanostructure aspect ratio results in ~20 nm increase in the difference between the minimized and maximized λ_{max} values.

In summary, optical characterization of extended nanostructures fabricated by performing multiple angle-resolved depositions on a single sample demonstrated diverse LSPR behavior. Polarized microextinction measurements probed the LSPR as a function of nanostructure orientation relative to the polarization of the incident light. In all cases, 180° symmetry was observed in plots of extent of rotation versus LSPR extinction maximum. This behavior is expected for nanoparticles with an effective long axis and short axis. The difference between the minimum LSPR λ_{max} (polarization

aligned with the short axis) and the maximum LSPR λ_{max} (polarization aligned with the long axis) is indicative of the effective aspect ratio of the multiple deposition nanostructures. Increasing effective aspect ratio of the four nanostructures proceeds in the following order: nanogaps, nanooverlaps, nanocontacts, and nanochains. The unexpectedly small effective aspect ratio of the nanogap structure can be attributed to the complicated nature of electromagnetic coupling when nanoparticles in close proximity are not in direct contact. These multiple deposition AR NSL structures hold significant potential as dichroic filters. In fact, the dichroic contrast measured with the nanochain nanostructures is the largest contrast demonstrated with noble metal nanoparticles to date.

Acknowledgment. We acknowledge support of the Nanoscale Science and Engineering Initiative of the National Science Foundation under NSF Award Number EEC-0118025. Any opinions, findings, and conclusions or recommendations expressed in this material are those of the author(s) and do not necessarily reflect those of the National Science Foundation. We also acknowledge the support of the Air Force Office of Scientific Research Multidisciplinary University Research Initiative program (Grant F49620-02-1-0381). C.L.H. acknowledges the support of a Northwestern University Presidential Fellowship.

References

(1) Wallraff, G. M.; Hinsberg, W. D. *Chem. Rev.* **1999**, *99*, 1801.
(2) Ito, T.; Okazaki, S. *Nature* **2000**, *406*, 1027.
(3) Bloomstein, T. M.; Horn, M. W.; Rothschild, M.; Kunz, R. R.; Palmacci, S. T.; Goodman, R. B. *J. Vac. Sci. Technol. B* **1997**, *15*, 2112.
(4) Liao, P. F.; Bergman, J. G.; Chemla, D. S.; Wokaun, A.; Melngailis, J.; Hawryluk, A. M.; Economou, N. P. *Chem. Phys. Lett.* **1981**, *81*, 355.
(5) Liao, P. F. Silver Structures Produced by Microlithography. In *Surface Enhanced Raman Scattering*; Chang, R. K., Furtak, T. E., Eds.; Plenum Press: New York, 1982; p 379.
(6) Howard, R. E.; Liao, P. F.; Skocpol, W. J.; Jackel, L. D.; Craighead, H. G. *Science* **1983**, *221*, 117.
(7) Kitson, S. C.; Barnes, W. L.; Sambles, J. R. *IEEE Phot. Technol. Lett.* **1996**, *8*, 1662.
(8) Smith, H. I.; Schattenburg, M. L. *IBM J. Res. Dev.* **1993**, *37*, 319.
(9) Gotschy, W.; Vonmetz, K.; Leitner, A.; Aussenegg, F. R. *Opt. Lett.* **1996**, *21*, 1099.
(10) Lu, A. H.; Lu, G. H.; Kessinger, A. M.; Foss, C. A. *J. Phys. Chem. B* **1997**, *101*, 9139.
(11) Al-Rawashdeh, N. A. F.; Sandrock, M. L.; Seugling, C. J.; Foss, C. A. *J. Phys. Chem. B* **1998**, *102*, 361.
(12) Dirix, Y.; Bastiaansen, C.; Caseri, W.; Smith, P. *Adv. Mater.* **1999**, *11*, 223.
(13) Fort, E.; Ricolleau, C.; Sau-Pueyo, J. *Nano Lett.* **2003**, *3*, 65.
(14) Hulteen, J. C.; Van Duyne, R. P. *J. Vac. Sci. Technol. A* **1995**, *13*, 1553.
(15) Haynes, C. L.; Van Duyne, R. P. *J. Phys. Chem. B* **2001**, *105*, 5599.
(16) Haynes, C. L.; McFarland, A. D.; Smith, M. T.; Hulteen, J. C.; Van Duyne, R. P. *J. Phys. Chem. B* **2002**, *106*, 1898.
(17) Hulteen, J. C. 1. Surface-Enhanced Hyper-Raman Spectroscopy. 2. Nanosphere Lithography. Ph.D. Thesis, Northwestern University, 1995.
(18) Jensen, T. R. Optical Characterization of Nanofabricated Silver Films: Surface Plasmon Resonance and Surface-Enhanced Spectroscopy. Ph.D. Thesis, Northwestern University, 1999.
(19) Jensen, T. R.; Duval Malinsky, M.; Haynes, C. L.; Van Duyne, R. P. *J. Phys. Chem. B* **2000**, *104*, 10549.
(20) Jensen, T. R.; Duval, M. L.; Kelly, L.; Lazarides, A.; Schatz, G. C.; Van Duyne, R. P. *J. Phys. Chem. B* **1999**, *103*, 9846.
(21) Jensen, T. R.; Schatz, G. C.; Van Duyne, R. P. *J. Phys. Chem. B* **1999**, *103*, 2394.
(22) Duval Malinsky, M. Localized Surface Plasmon Resonance Spectroscopy of Silver Nanoparticles and Raman Spectroscopy Using Liquid-Core Optical Fibers: Fundamentals and Applications. Ph.D. Thesis, Northwestern University, 2000.
(23) Duval Malinsky, M.; Kelly, L.; Schatz, G. C.; Van Duyne, R. P. *J. Phys. Chem. B* **2001**, 2343.
(24) Duval Malinsky, M.; Kelly, L.; Schatz, G. C.; Van Duyne, R. P. *J. Am. Chem. Soc.* **2001**, *123*, 1471.
(25) Haynes, C. L.; McFarland, A. D.; Zhao, L.; Van Duyne, R. P.; Schatz, G. C.; Gunnarsson, L.; Prikulis, J.; Kasemo, B.; Käll, M. *J. Phys. Chem. B* **2003**, *107*, in press.

NL0342287